MAMERN VI–2015: 6^{th} International Conference on Approximation Methods
and Numerical Modelling in Environment and Natural Resources
Pau (France), June 1-5, 2015

A global reactive transport model applied to the MoMaS benchmark

Jocelyne Erhel [1] **and Souhila Sabit** [1]

[1] Inria
Campus de Beaulieu, 35042 Rennes Cedex, France
{jocelyne.erhel}@inria.fr; sabitsouhila@yahoo.fr

Keywords: geochemistry, transport, global method, MoMaS benchmark.

Abstract. *Reactive transport models are very useful for groundwater studies such as water quality, safety analysis of waste disposal, remediation, and so on. The MoMaS group defined a benchmark with several test cases. We present results obtained with a global method and show through these results the efficiency of our numerical model.*

1 Introduction

It is quite challenging to develop a numerical model for deep storage of nuclear waste. The time interval is very large (several thousands years), models are coupled and simulations must be accurate enough to be used for risk assessment. In most cases, chemistry must be included in models of deep geological storage. In addition to radioactive decay, chemical phenomna are numerous and include aqueous reactions, oxydo-reduction reactions, precipitation and dissolution reactions, ions exchanges, surface exchanges. These reactions can be either kinetic or at equilibrium.

Models must handle species which are in groundwater systems and take into account the mobile property of these species. It is thus necessary to consider a coupled model, where chemistry equations and radioactive decay are

combined with transport of contaminants. These models are partial differential equations (for transport, one equation for each species), and algebraic or differential equations (for chemistry, a system at each grid point).

The MoMaS benchmark was designed as a set of academic examples, in order to run experiments with several methods and software [3], [4]. Several authors participated in the exercise [1], [7], [12],[13], [14]. A synthetic comparison of their results indicate that, for this benchmark, the fastest results were obtained with global approaches [2].

In this paper, we show original results obtained with a global approach for the so-called 2D easy test case of the MoMaS benchmark. The model proposed in MoMaS is based on the introduction of total analytical concentrations, thanks to the linearity of the transport equation. It is a set of Partial Algebraic Differential Equations. We use the method developed in [6, 8] and improved in [9, 17]. In this method, we first discretize in space, using a Finite Difference scheme, then we discretize in time, using an implicit BDF scheme. Thus at each time step, we have to solve nonlinear equations which we keep coupled.

Compared with [8], we bring three improvements in [9, 17]. First, we use a substitution technique, similar do global DSA methods, which allows reducing the size of nonlinear systems. We still keep the differential variables in the semi-discrete system, in order to use adaptive time steps and adaptive Jacobian updates. Logarithmic variables are very convenient to ensure the positivity of the concentrations and to compute the derivatives, but they can lead to severely ill-conditioned Jacobian matrices [17]. Thus, our second improvement consists in using non logarithmic variables, at the price of ensuring positivity during nonlinear iterations. In the benchmark, the first component is inert, so our third improvement is to remove this component from the coupled equations.

The paper is organized as follows. In section 2, we describe the mathematical model of the MoMaS test case studied and provide our simulation results for flow and transport of the five main species. The numerical method is defined in section 3, as well as three versions of our software GRT3D [17]. Finally, we analyse in section 4 the efficiency of the improvements brought to the original global method. We discuss these results and outline future work in the concluding section 5.

2 MoMaS benchmark

The MoMaS group studies mathematical models and numerical simulations for nuclear waste disposal. A set of test cases were defined for transport reactive problems [4]. Here, we make experiments with the so-called easy test case, in 2D. The computational domain is a rectangle with two porous media, see Fi-

gure 1. All dimensions are normalized, with length unit L and time unit T.

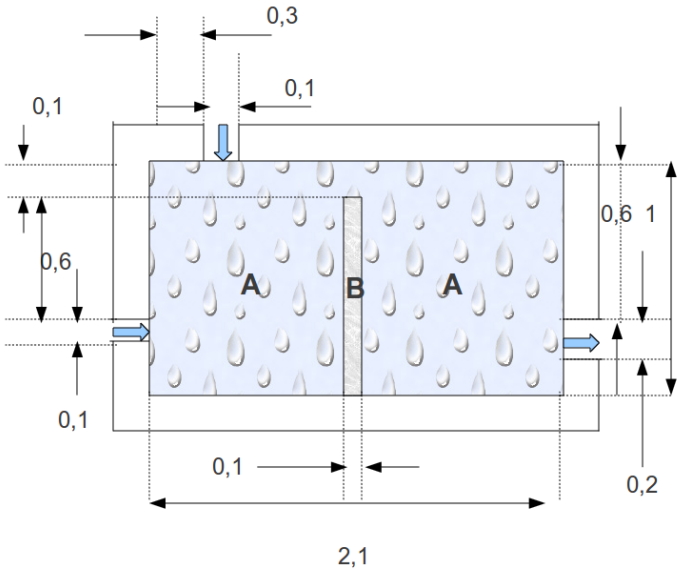

FIGURE 1: Computational domain for MoMaS Benchmark (dimensions are in the unit length L).

2.1 Flow simulations

The benchmark considers a steady saturated one-phase flow, with no source term. Flow is governed by Darcy's law and mass conservation, giving mathematical equations (1) where the pressure h and the Darcy's velocity q are the unknowns and $\mathbf{K}$ is the hydraulic conductivity.

$$\begin{cases} q = -\mathbf{K}\nabla h, \\ \nabla q = 0. \end{cases} \tag{1}$$

Darcy's velocity is related to the porosity ε and to the pore velocity v by $q = \varepsilon v$.

Medium A has a high conductivity and a low porosity, whereas medium B has a low conductivity and a high porosity, see Table 1.

Boundary conditions must be prescribed to complete the PDE system. At outflow, the pressure is given by $h = 1L$. At both inflows, the flow velocity is given by $q = 2.25 \times 10^{-2} L.T^{-1}$, whereas no flow condition is applied at other boundaries.

	Medium A	Medium B
Porosity ε	0.25	0.5
Conductivity K (L.T^{-1})	10^{-2}	10^{-5}

TABLE 1: Flow conditions for MoMaS benchmark.

We simulate the flow equations with the software MODFLOW [10]. Figures 2 et 3 show the velocity and the pressure computed with a mesh of 40×84 cells [6], [17].

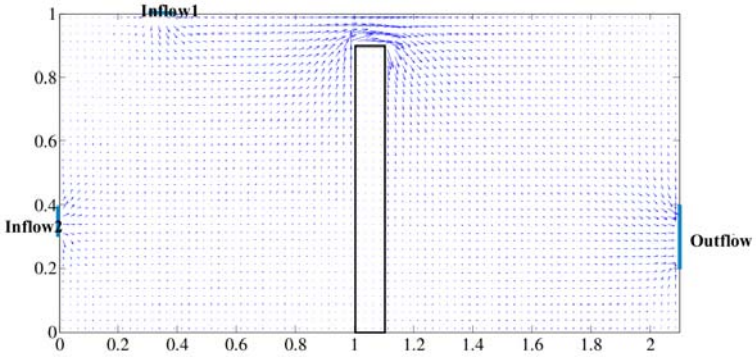

FIGURE 2: Velocity field with a mesh of 40×84 cells.

2.2 Transport simulations

Transport of mass in groundwater is governed by advection and dispersion. There is no source term in the benchmark test. The concentration c of an inert solute is the solution of the PDE (2) expressing a mass conservation law.

$$\varepsilon\frac{\partial c}{\partial t} = \nabla.(D\ \nabla c) - \nabla.(q\ c), \tag{2}$$

where the dispersion tensor D is given by

$$D = \varepsilon d_m I + \alpha_T \|q\| I + (\alpha_L - \alpha_T)\frac{qq^T}{\|q\|}.$$

We consider the advective test case of the MoMaS benchmark, without molecular diffusion, see Table 2.

Initial conditions at time $t = 0T$ are applied to the geochemistry system, see Table 5. The final time is $t = 6000T$.

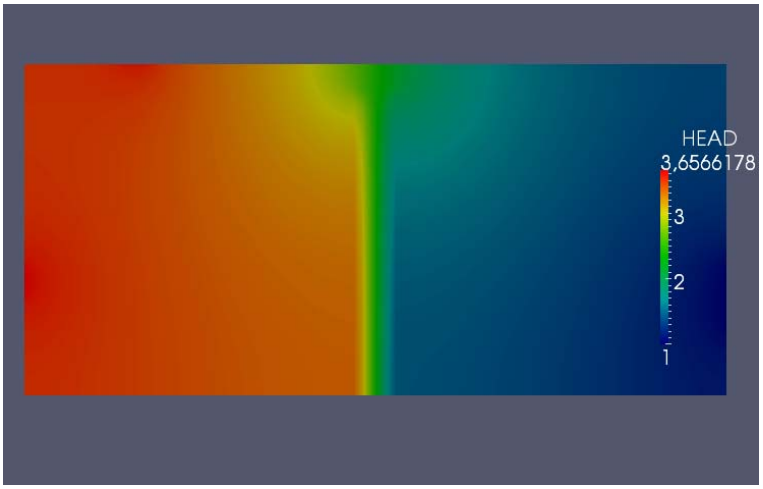

FIGURE 3: Pressure head with a mesh of 40×84 cells.

	Medium A	Medium B
Molecular diffusion d_m (L^2T^{-1})	0	0
Longitudinal Dispersion $\alpha_L(L)$	10^{-2}	6×10^{-2}
Transverse Dispersion $\alpha_T(L)$	10^{-3}	6×10^{-3}

TABLE 2: Transport conditions for benchmark MoMaS.

At impermeable boundaries, a no total flux condition is imposed. At ouflow, a zero concentration gradient is imposed. At both inflows, concentration is prescribed, with values given in Table 6. Injection occurs during a first period of time until $t = 5000T$, followed by a leaching period until the end.

The first chemical component is a spectator ion, which behaves like a inert solute. For this component, we can simulate the transport equations with the software MT3D [18]. Figure 4 represents the concentration at various times, obtained with a fine mesh of 80×168 cells.

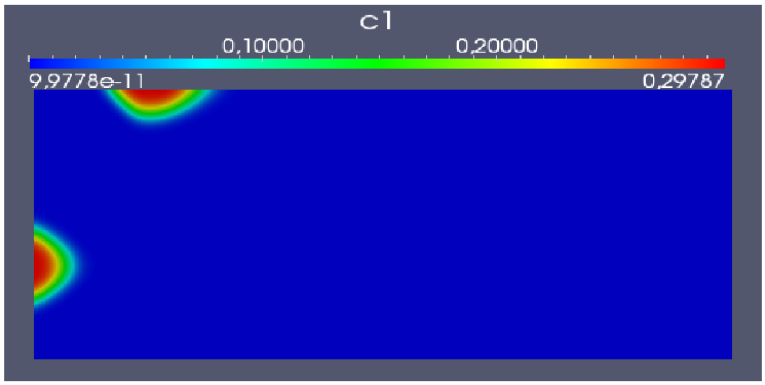

(a) Time $t = 1T$

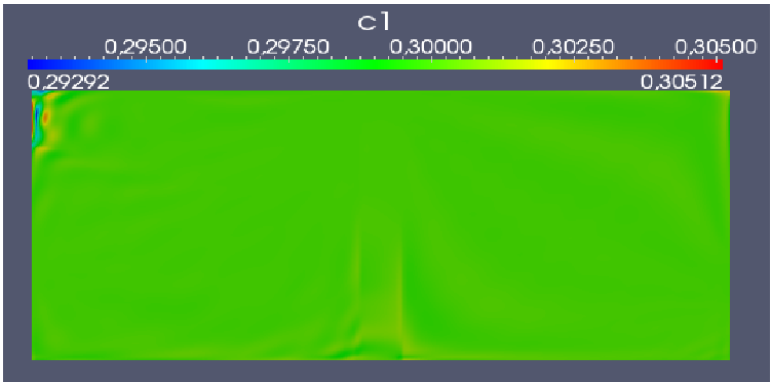

(b) Time $t = 4000T$

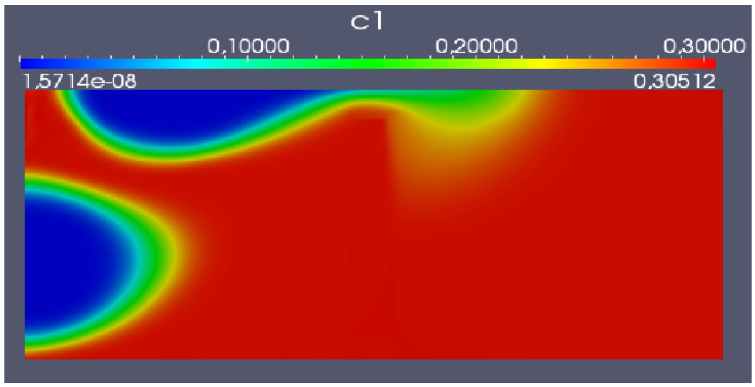

(c) Time $t = 5010T$

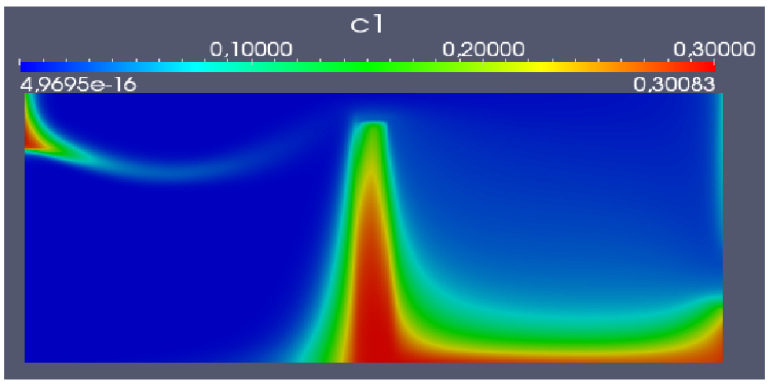

(d) Time $t = 5800T$

FIGURE 4: Concentrations of the inert solute c_1 at different times (with different scales).

2.3 Geochemistry simulations

In the MoMaS test case, the geochemical system has $N_c = 4$ aqueous components c_j and $N_s = 1$ fixed component s_j. They react with $N_\alpha = 5$ aqueous secondary species α_i and $N_\beta = 2$ fixed secondary species β_i. There is no precipitation dissolution. All the activities are equal to 1 and the variables $c_j, s_j, \alpha_i, \beta_i$ are the concentrations of the species.

Stoichiometric coefficients and equilibrium constants are given in Table 3. In the original benchmark, the constant K_{c5} is equal to 10^{+35} but we replace it by 10^{+6}. Indeed, with such a very large constant, the chemical nonlinear system is highly ill-conditioned and numerical simulations can suffer from strong inaccuracies.

	c_1	c_2	c_3	c_4	s	K
α_1	0	-1	0	0	0	10^{-12}
α_2	0	1	1	0	0	1
α_3	0	-1	0	1	0	1
α_4	0	-4	1	3	0	0.1
α_5	0	4	3	1	0	10^{+6}
β_1	0	3	1	0	1	10^{+6}
β_2	0	-3	0	1	2	10^{-1}

TABLE 3: Stoichiometric coefficients and equilibrium constants for MoMaS benchmark (with K_{c5} modified).

Table 3 is summarized in Table 4 by using algebraic notations, with the matrices S, A, B and the vectors $c, s, \alpha, \beta, K_c, K_s$.

	c	s	K
α	S	0	K_c
β	A	B	K_s

TABLE 4: Algebraic representation of Table 3.

Secondary species can be computed thanks to the mass action laws (3) describing the chemical reactions. Moreover, the concentrations of the compo-

nents must be positive.

$$\begin{cases} \alpha_i(c) = K_{ci} \prod_{j=1}^{N_c} c_j^{S_{ij}}, \quad i = 1, \dots N_\alpha, \\ \beta_i(c,s) = K_{si} \prod_{j=1}^{N_c} c_j^{A_{ij}} \prod_{j=1}^{N_s} s_j^{B_{ij}}, \quad i = 1, \dots N_\beta, \\ c_j \geq 0, \quad j = 1, \dots N_c, \\ s_j \geq 0, \quad j = 1, \dots N_s. \end{cases} \tag{3}$$

Then the model applies the mass conservation law to the chemical system.

$$\begin{cases} c + S^T \alpha(c) + A^T \beta(c,s) = T, \\ s + B^T \beta(c,s) = W, \end{cases} \tag{4}$$

where T and W are respectively the total analytical concentrations for mobile and fixed components. In a closed system, these quantities are known, but they vary in time and space when the species are transported by water.

2.4 Reactive transport

Transport is now governed not only by advection and dispersion, but also by reaction. A mass conservation equation can be written for each component and each secondary species, where the reaction terms are unknowns in the context of reactions at equilibrium. However, because the dispersion tensor is the same for all the species, the transport terms are linear and it is possible to compute a linear combination of all the equations. This ends up to mass conservation equations (5) applied to the total analytical concentrations T, where the reaction terms cancel and disappear. Moreover, the total analytical concentrations W remain constant and given.

$$\varepsilon \frac{\partial T_j}{\partial t} = \nabla.(D\, \nabla C_j(c)) - \nabla.(q\, C_j(c)),\ j = 1, \dots N_c, \tag{5}$$

where $C(c) = c + S^T \alpha(c)$ is the total mobile concentration.

Equations (5) are coupled with the mass action laws (3) and the mass conservation laws (4) written at each point of the computational domain.

Initial conditions for the 5 components are given in Table 5. It can be noted that $T_3 = 0$ implies that $c_3 = \alpha_2 = \alpha_4 = \alpha_5 = \beta_1 = 0$, because all the associated stoichiometric coefficients are strictly positive. Therefore, the equilibrium constants $K_{c2}, K_{c4}, K_{c5}, K_{s1}$ have to mathematical effect on the initial equilibrium. However, they may have a numerical effect.

Boundary conditions at both inflows are given in Table 6 for the injection and leaching periods. Again, it can be noted that $T_3 = 0$ during the leaching period, and $T_4 = 0$ during the injection period. Since the stoichiometric coefficients associated to c_4 are also strictly positive, $c_4 = \alpha_3 = \alpha_4 = \alpha_5 =$

$\beta_2 = 0$ during the injection period. Thus, at inflow, the equilibrium constants K_{c4}, K_{c5}, K_{s2} have to mathematical effect on the equilibrium.

	T_1	T_2	T_3	T_4	W
Medium A	0	-2	0	2	1
Medium B	0	-2	0	2	10

TABLE 5: Initial conditions for MoMaS benchmark.

	T_1	T_2	T_3	T_4	W
Injection $t \in [0, 5000]$	0.3	0.3	0.3	0	0
Leaching $t \in [5000, 6000]$	0	-2	0	2	0

TABLE 6: Inflow conditions for MoMaS benchmark.

Figures 5 to 10 show the concentrations of the aqueous components c_2, c_3, c_4 and the fixed component s at various times. They cannot be compared exactly to the results of the literature [3, 12, 13, 14], because we changed the constant K_{c5}, but they are very close.

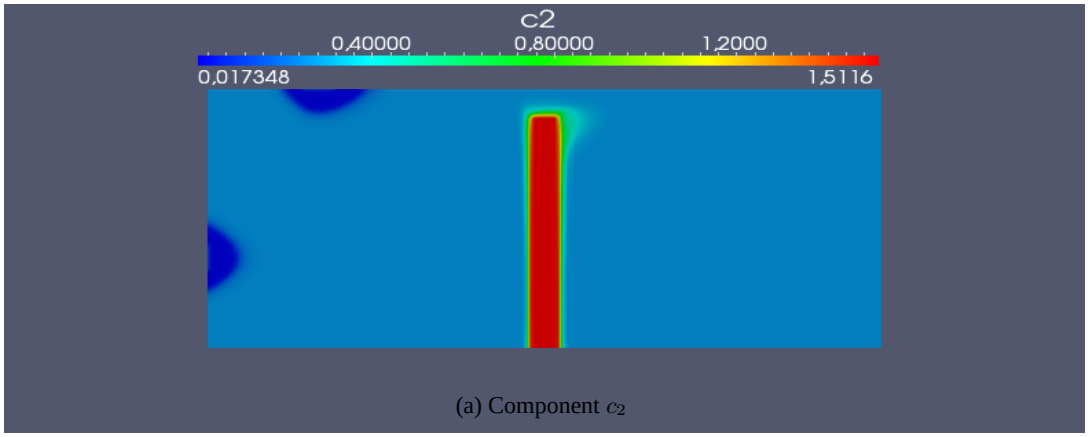

(a) Component c_2

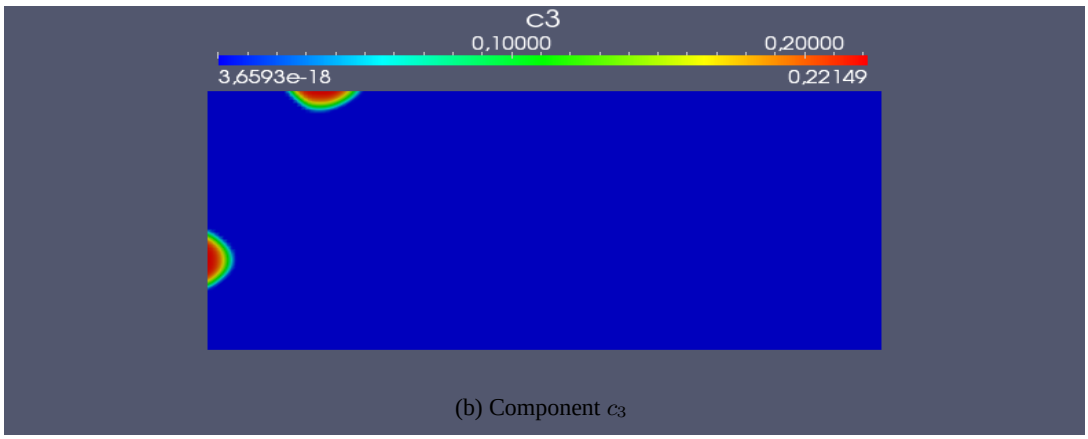

(b) Component c_3

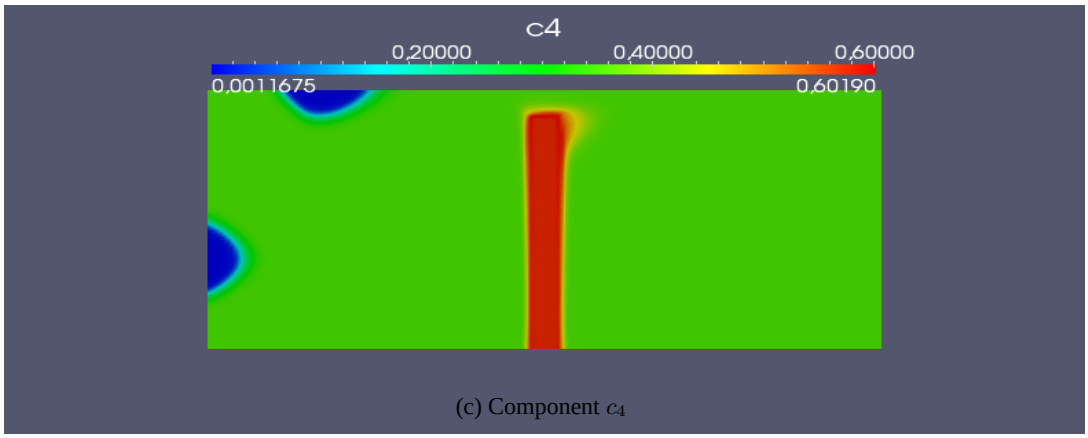

(c) Component c_4

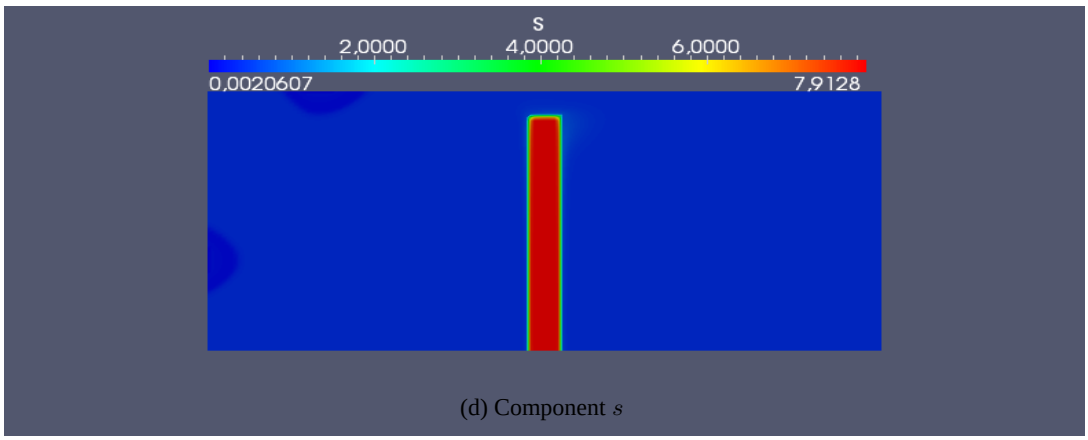

(d) Component s

FIGURE 5: Concentrations of the four reactive components at time $t = 10T$.

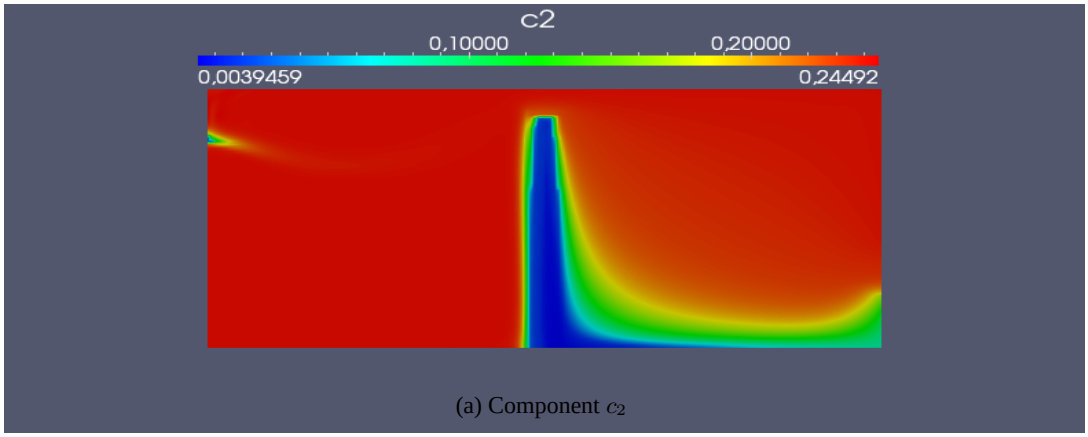

(a) Component c_2

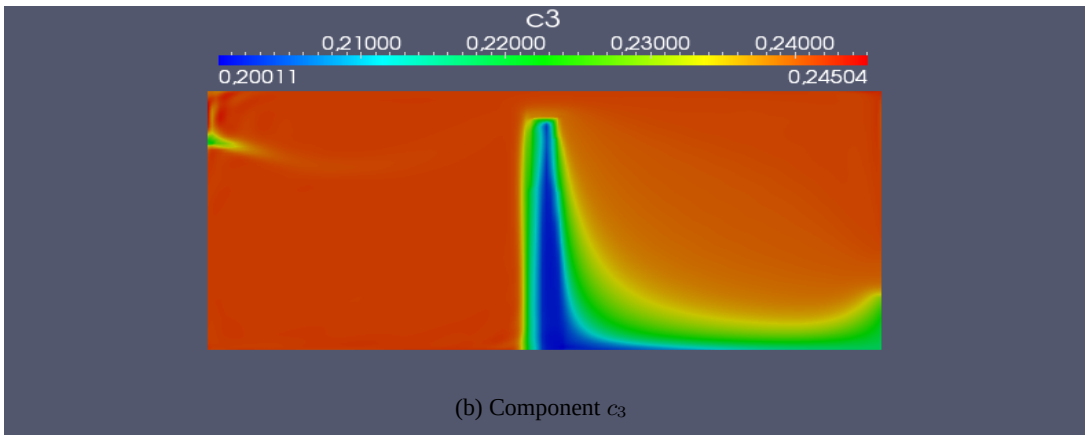

(b) Component c_3

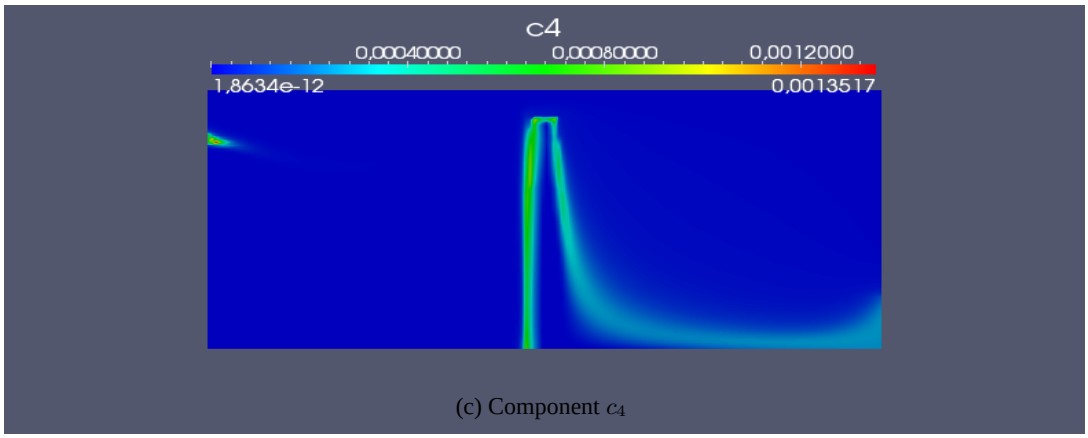

(c) Component c_4

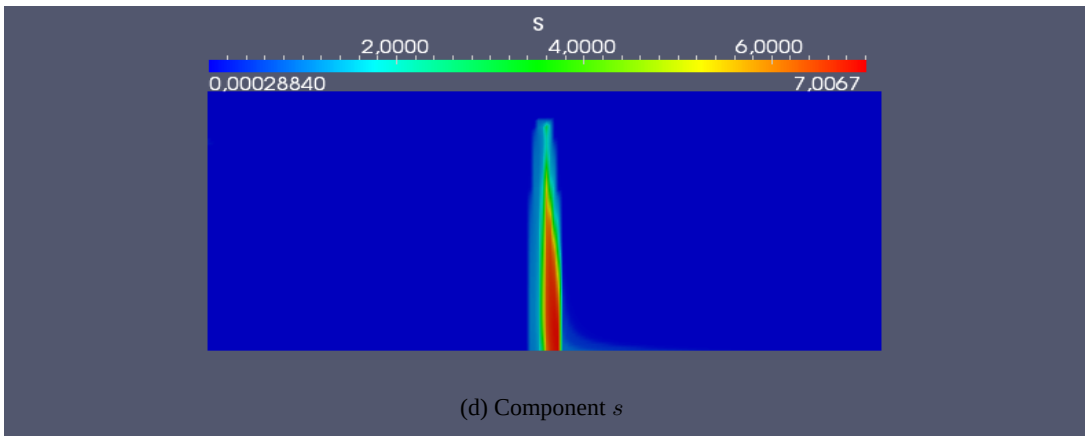

(d) Component s

FIGURE 6: Concentrations of the four reactive components at time $t = 2000T$.

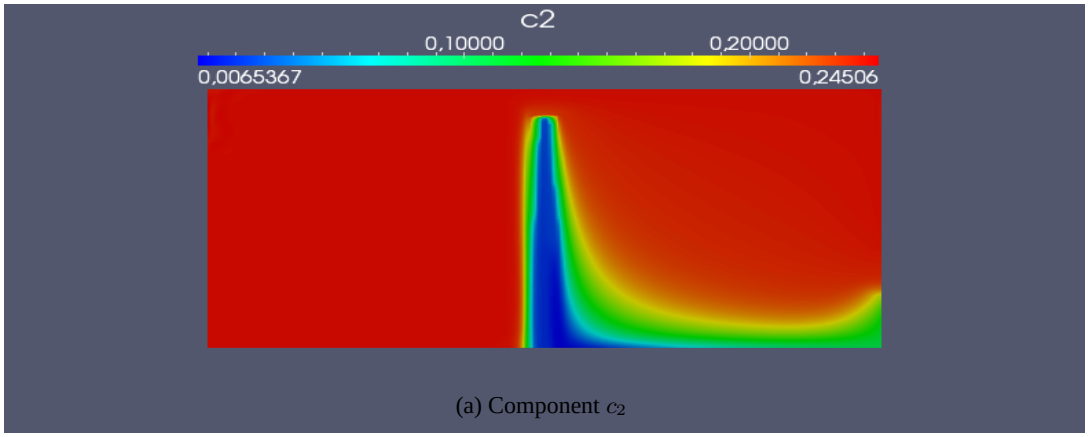

(a) Component c_2

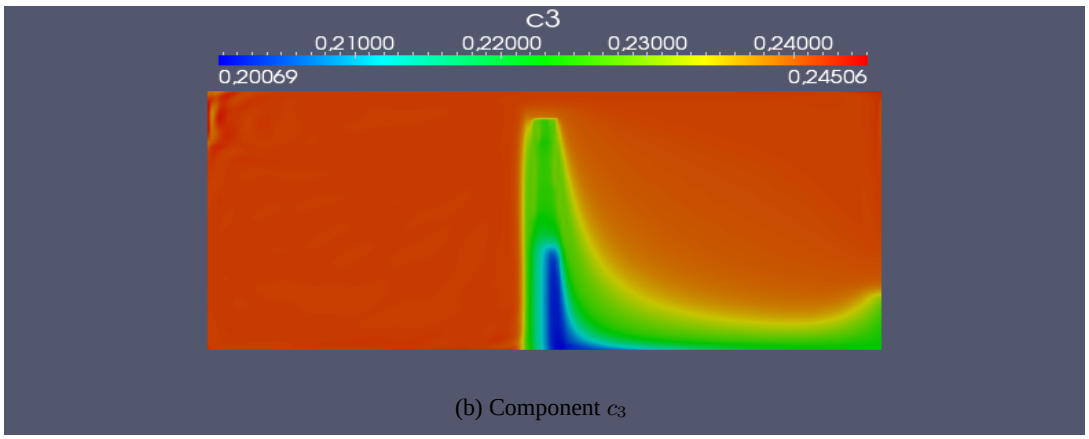

(b) Component c_3

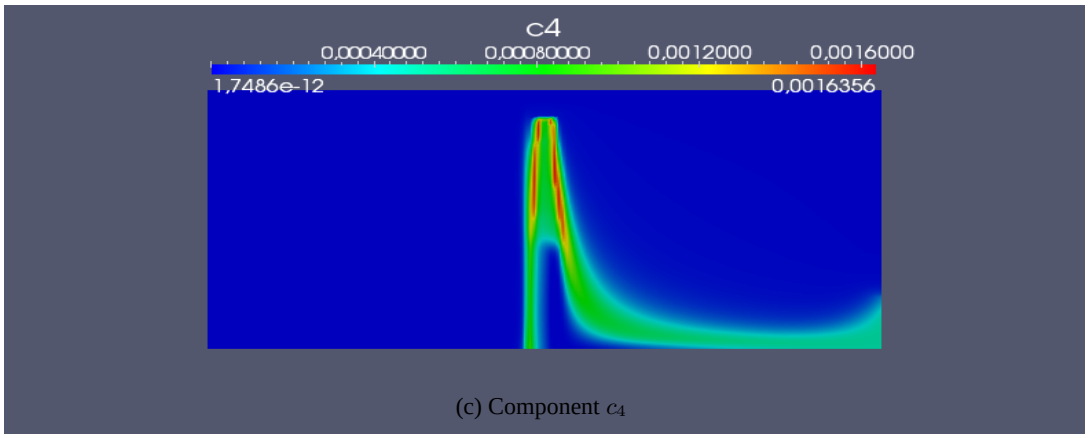

(c) Component c_4

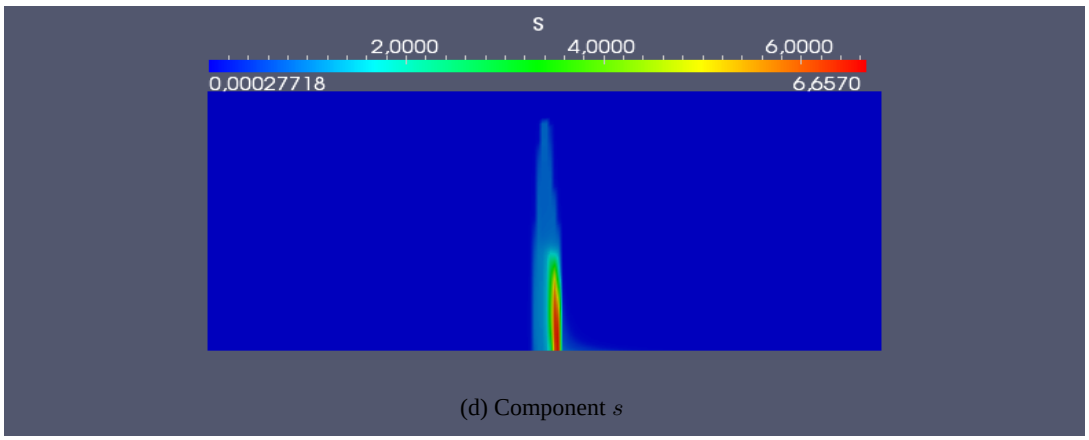

(d) Component s

FIGURE 7: Concentrations of the four reactive components at time $t = 4000T$.

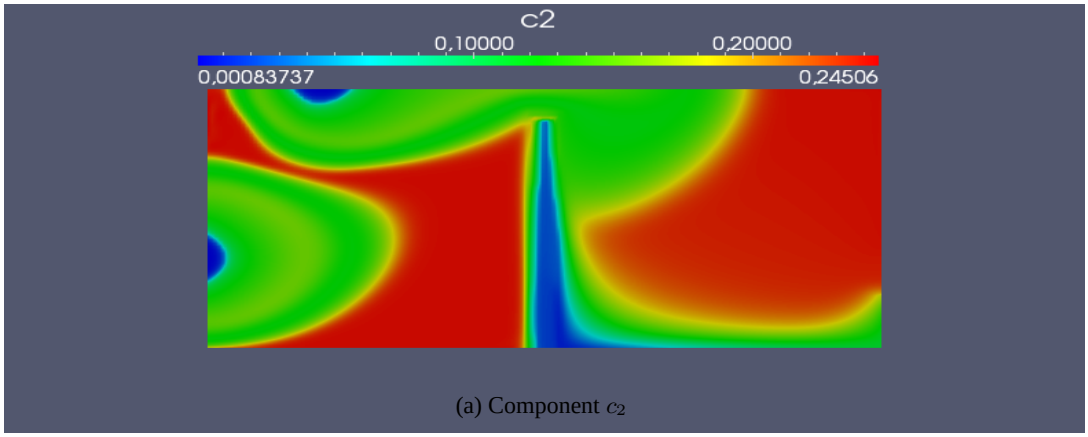

(a) Component c_2

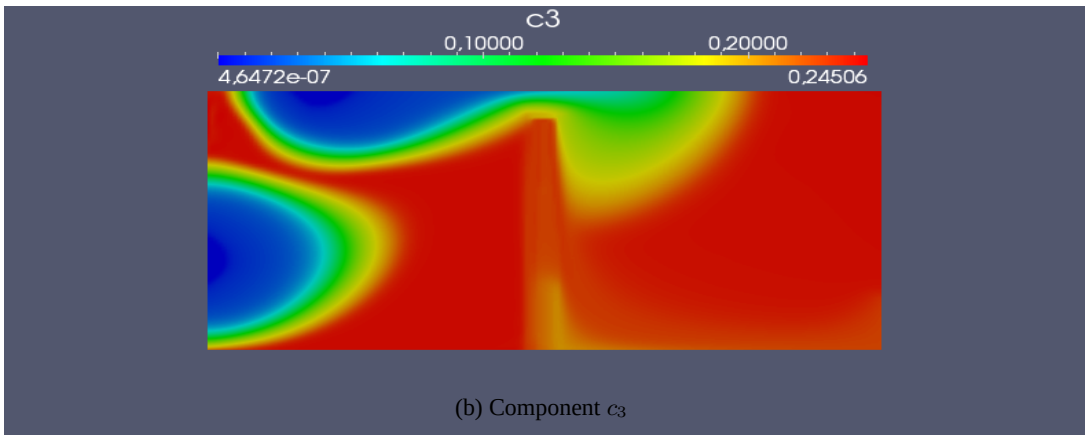

(b) Component c_3

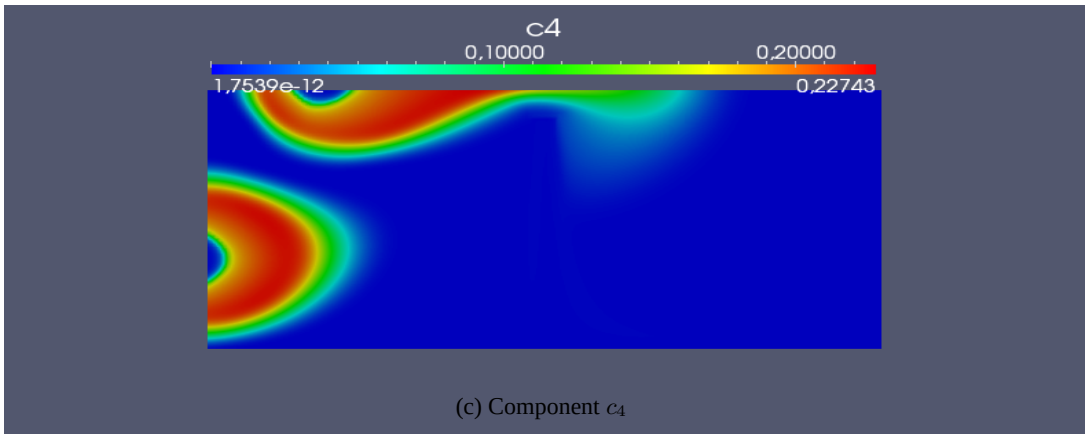

(c) Component c_4

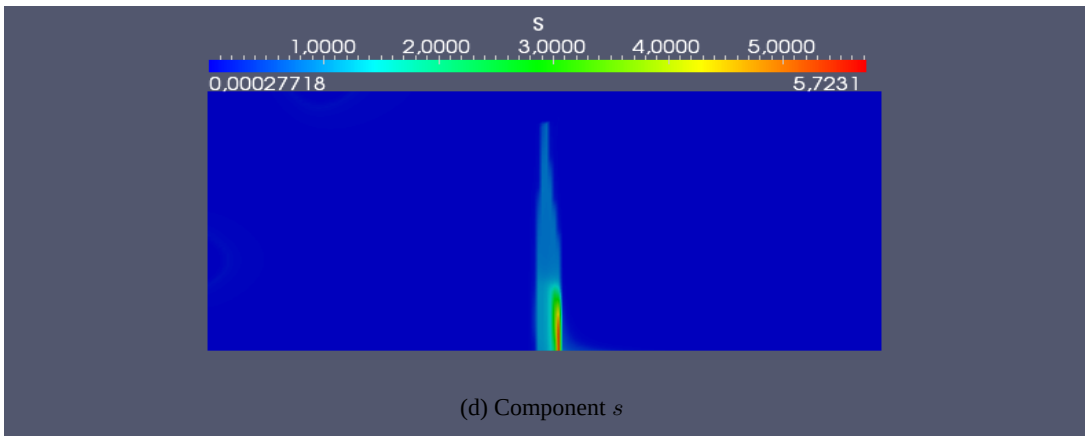

(d) Component s

FIGURE 8: Concentrations of the four reactive components at time $t = 5010T$.

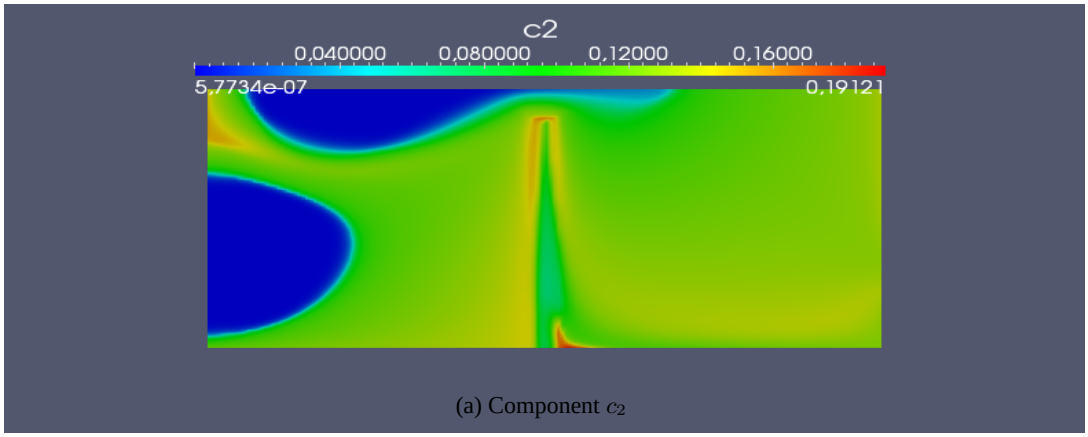

(a) Component c_2

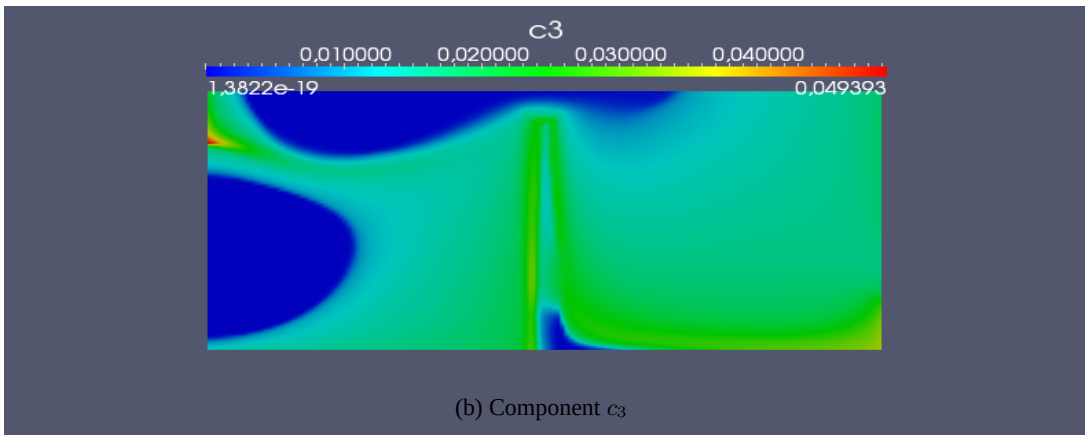

(b) Component c_3

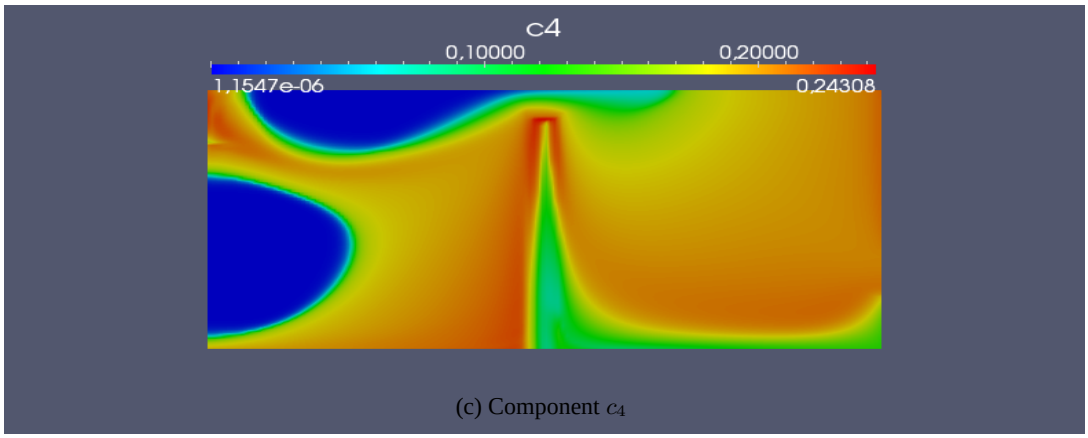

(c) Component c_4

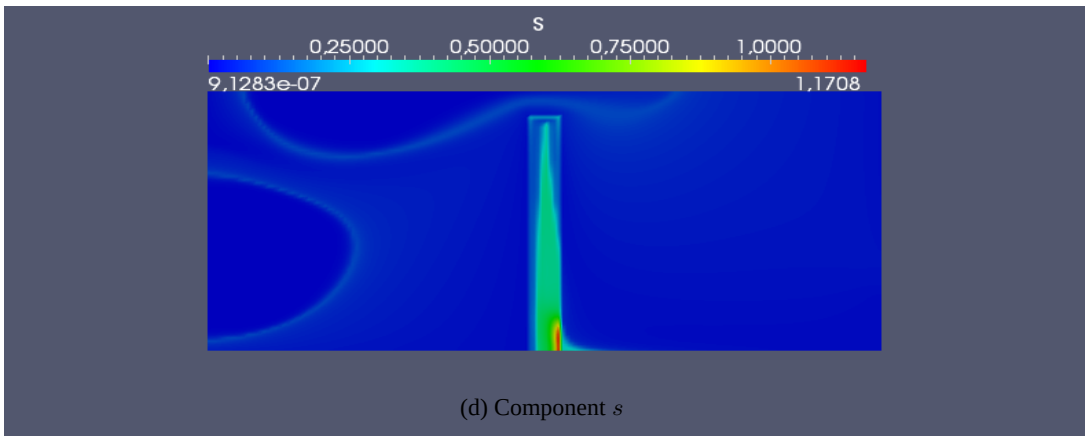

(d) Component s

FIGURE 9: Concentrations of the four reactive components at time $t = 5200T$.

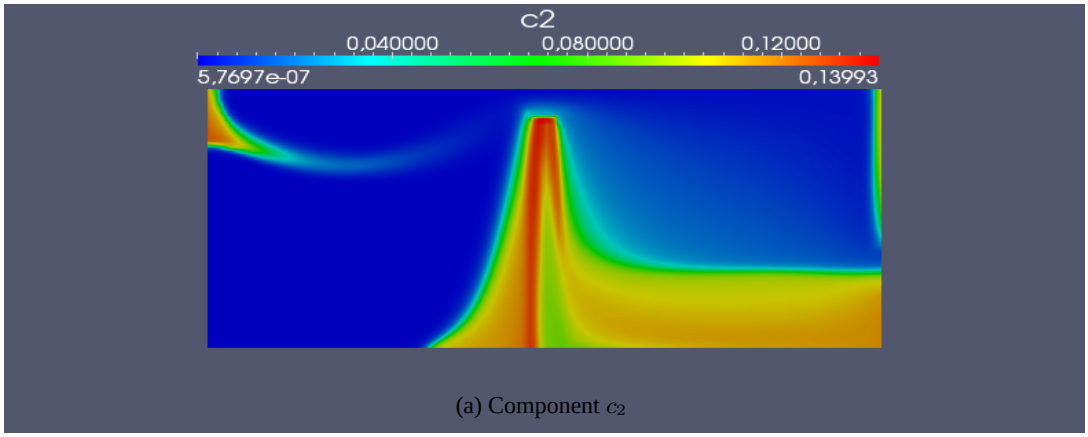

(a) Component c_2

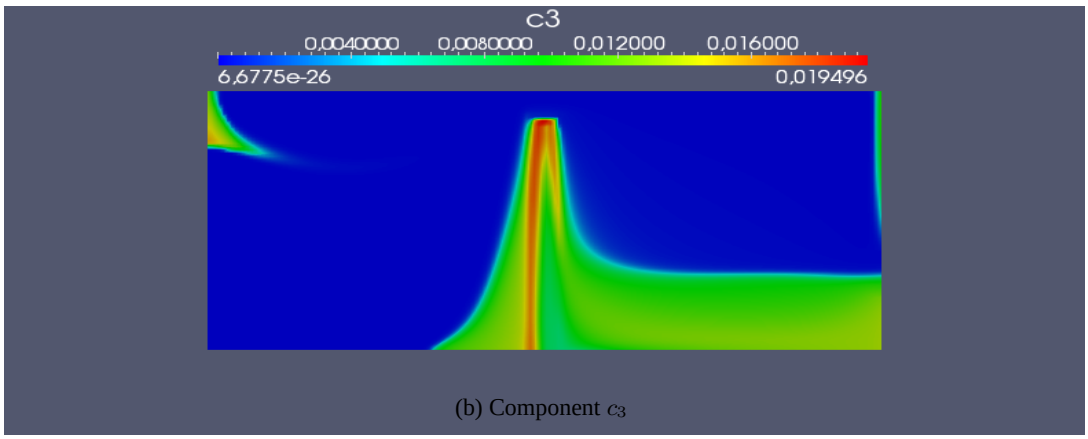

(b) Component c_3

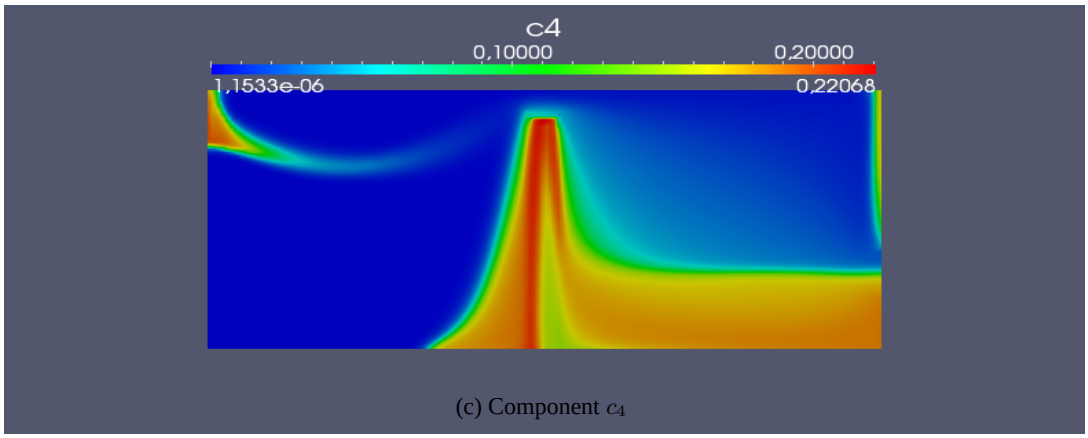

(c) Component c_4

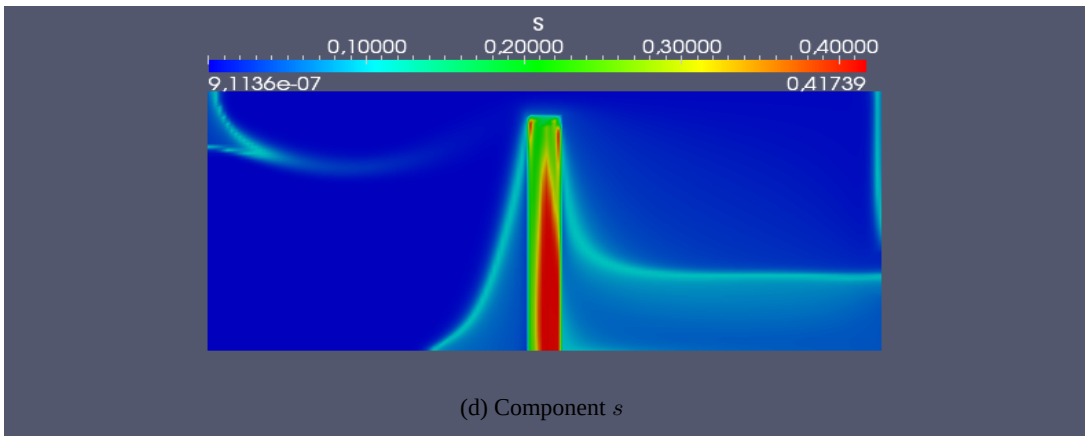

(d) Component s

FIGURE 10: Concentrations of the four reactive components at time $t = 5800T$.

3 Numerical method

Equations (3),(4),(5) form a PDAE system composed of algebraic and PDE equations. We assume that it is well-posed.

Following a method of lines, we first discretize in space, using a finite difference scheme implemented in the software MT3D. We define a regular mesh of the domain with a rectangle of $N_x \times N_y$ cells. We get a DAE semi-discrete system, where the algebraic chemistry equations are written at each point of the mesh [6, 8].

Because the system is stiff, we use an implicit scheme, involving a global nonlinear system at each time step, coupling transport and chemistry equations. We use a BDF scheme implemented in the software SUNDIALS [11]. At each time step, the nonlinear system is solved with a Newton's method. We provide the function of the DAE equation and its derivative, whereas the module IDA of SUNDIALS provides the implicit scheme.

Time discretization comes with an adaptive time step, which controls both the accuracy of the approximation and the convergence of Newton's iterations. It allows choosing large time steps when possible and saves CPU time.

We solve the linearized equations with a sparse direct solver, implemented in the software library UMFPACK [5], which we have interfaced with SUNDIALS. We thus factorize the Jacobian matrix and use the triangular factors to solve the linearized equations. The software keeps the Jacobian of linearized Newton's iterations frozen while convergence is fast enough, saving updates and factorizations thus CPU time.

We implemented three versions of our method in the software suite GRT3D [9, 17]. Mass action laws can be linearized by introducing logarithmic variables, if they are strictly positive. In a first version, called GRT3D, we used as primary variables the total T, the total mobile C and the components concentrations $\log(c), \log(s)$. In a second version, called GRT3DRL, we reduced the size of linearized systems by using a substitution approach, keeping only the variables $\log(c), \log(s)$ in the linear systems to be solved. This technique saves CPU time by factorizing a smaller matrix. In a third version, called GRT3DRSL, we used the same algorithms, but with the non logarithmic variables c, s.

4 Performance analysis

In this section, we analyze the computational time of our simulations. All experiments are done in sequential, on a Intel Xeon computer, with 24 MB of RAM and with 12 MB of cache memory.

We compare the three versions of our software : GRT3D uses logarithms

and no substitution, GRT3DRL still uses logarithms but eliminates unknowns T and C in the linearized systems, GRT3DRSL does not use logarithms and applies substitution. Also, we can remove the first component c_1 since it is inert so we can further reduce the system size.

Simulations are done with three different meshes, a coarse mesh with $N_m = 20 \times 42$ cells, an intermediate mesh with $N_m = 40 \times 84$, and a fine mesh with $N_m = 80 \times 168$ cells.

4.1 CPU time

Mesh	GRT3D	GRT3DRL
20x42	10920	4200
40x84	43680	16800
80x168	174720	67200

TABLE 7: System size using GRT3D and GRT3DRL with the first inert component.

Mesh	GRT3D	GRT3DRL
20x42	8400	3360
40x84	33600	13440
80x168	134400	53760

TABLE 8: System size using GRT3D and GRT3DRL without the first inert component.

The reduction of the system size is given in Tables 7 and 8, respectively with the first inert component and without it. With the inert component, the system size is reduced from $(3N_c + N_s) \times N_m = 13N_m$ in GRT3D to $(N_c + N_s) \times N_m = 5N_m$ in GRT3DRL and GRT3DRSL. Without the inert component, reduction is from $10N_m$ to $4N_m$.

Clearly, reducing the system size has a direct impact on the CPU time. The total CPU time for the three versions is given in Table 9 for computations with the first inert component and in Table 10 without it.

CPU time decreases also when variables are not logarithmic. In order to analyze these effects, we use the measures taken at each external timestep of the software SUNDIALS. In Figure 11, we plot the CPU time versus the simu-

Mesh	GRT3D	GRT3DRL	GRT3DRSL
20x42	52 m 52 s	27 m 16 s	19 m 6 s
40x84	9 h 52 m 24 s	4 h 44 m 40 s	3 h 9 m 8 s
80x168	5 j 15 h 12 m 15 s	3 j 11 h 24 m 23 s	2 j 2 h 12 m 5 s

TABLE 9: CPU time of the three versions with the first inert component.

Mesh	GRT3D	GRT3DRL	GRT3DRSL
20x42	40 m 20 s	19 m 1 s	13 m 49 s
40x84	7 h 20 m 22 s	4 h 4 m 1 s	2 h 12 m 45 s
80x168	2 j 18 h 22 m 46 s	2 j 6 h 56 m 42 s	1 j 8 h 20 m 46 s

TABLE 10: CPU time of the three versions without the first inert component.

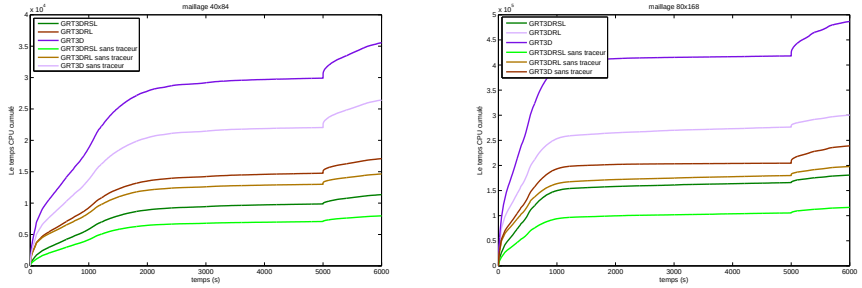

(a) Intermediate mesh (b) Fine mesh

FIGURE 11: CPU time during the simulation for the six variants.

lated time, for the six simulations (three versions of software, with and without the first component), and for two grids (intermediate mesh and fine mesh). During all the simulated time interval, the substitution approach, as well as the elimination of the first component, reduce the CPU time. Also, the use of non logarithmic variables is much more efficient.

For all the simulations, the CPU time increases rapidly until about $t = 1800T$ for the intermediate mesh and $t = 1000T$ for the fine mesh. Then it levels off until time $t = 5000T$ and increases again rapidly when the inflow boundary conditions change. We analyse the outputs of the software IDA in order to explain this behavior.

4.2 Effect of adaptive time step

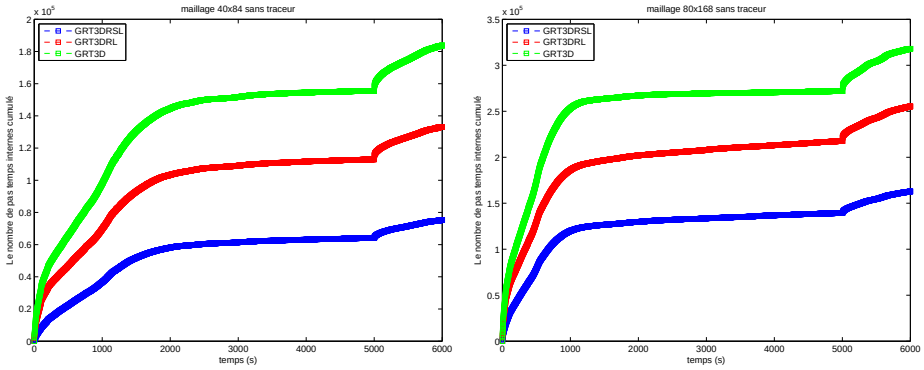

(a) Intermediate mesh (b) Fine mesh

FIGURE 12: Number of time steps during the simulation (different scales).

The IDA solver in the software SUNDIALS adjusts automatically the time step, in order to control both the accuracy of time discretization and the convergence of Newton's iterations. In Figure 12, we plot the number of time steps taken during the whole simulation. Here, we show only results without the first component, since results with this component are very similar.

As expected, the CPU time is strongly correlated with the number of time steps. The initial and boundary conditions are difficult to handle and require small time steps during a period of time until larger time steps can be taken. It takes more time with the intermediate mesh than with the fine mesh, probably because the sharp fronts of concentrations are better captured with the fine mesh. Anyway, these results demonstrate the efficiency of adaptive time step.

4.3 Effect of modified Newton's iterations

The number of time steps has a direct impact on the number of Newton's iterations which can be measured by the number of linear system solvings. It is also correlated to the number of updates of the Jacobian matrix, which can be measured by the number of matrix factorizations. Indeed, in our simulations, we use a direct sparse linear solver implemented in the software UMFPACK. Thus each time the Jacobian is updated, it has to be factorized in order to solve the linear systems associated to this new Jacobian.

In Figure 13, we plot the number of linear solvings and matrix factoriza-

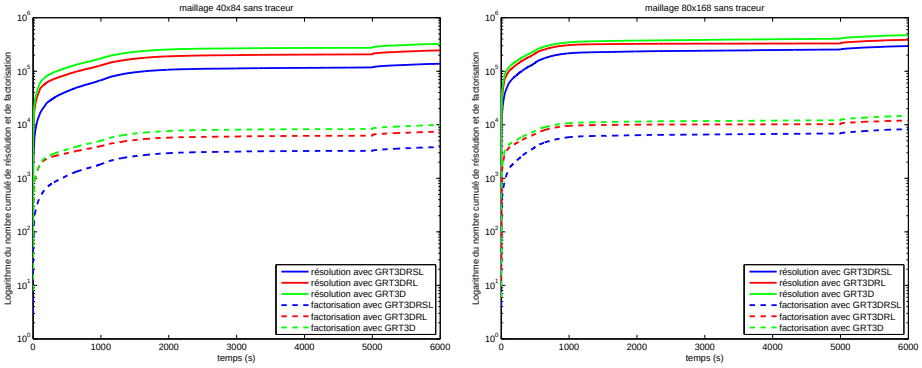

(a) Intermediate mesh (b) Fine mesh

FIGURE 13: Number of linear solvings and matrix factorizations during the simulation (logarithmic scale).

tions, for the three versions and for two meshes. Theses numbers are in logarithmic scale. Here, the first component is not considered, similar results are obtained when including it.

Again, we observe a sharp increase of these numbers at the beginning of the simulation and a small jump after leaching. At time $t = 0$, the number of solvings as well as the number of factorizations are slightly smaller when reducing the system size, from GRT3D to GRT3DRL. They are clearly smaller when using non logarithmic variables. This result is probably due to a better condition number of the Jacobian matrix at time $t = 0$.

For the three versions, the number of matrix factorizations is much smaller than the number of linear system solvings. This result demonstrates the efficiency of adaptive modified Newton's iterations. Indeed, the Jacobian is kept frozen during several time steps and during nonlinear iterations, so that factorization does not occur as often as solving.

4.4 Algorithmic complexity of Newton's iterations

It is well-known that the algorithmic complexity of sparse matrix factorization is much higher than the complexity of sparse system solving, which involves sparse triangular matrices. Thus, in order to fully measure the efficiency of the adaptive update of the Jacobian matrix, we have to analyze the CPU time of the Newton's iterations.

In Figure 14, we plot the CPU time (in logarithmic scale) of the linear

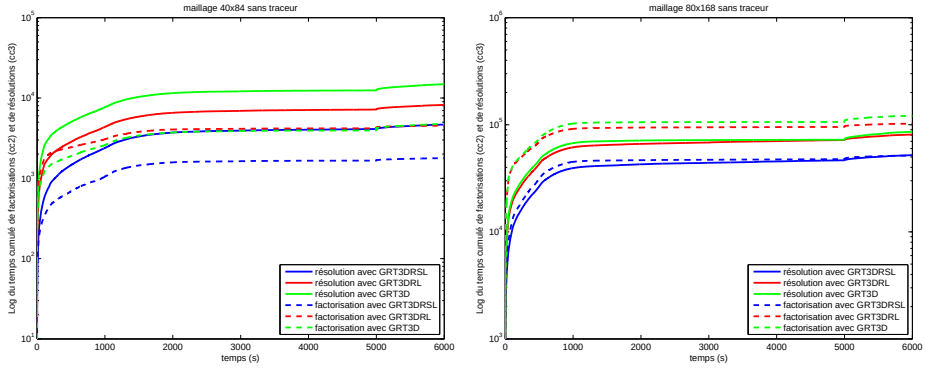

(a) Intermediate mesh (b) Fine mesh

FIGURE 14: CPU time during the simulation of the linear system solvings and the matrix factorizations.

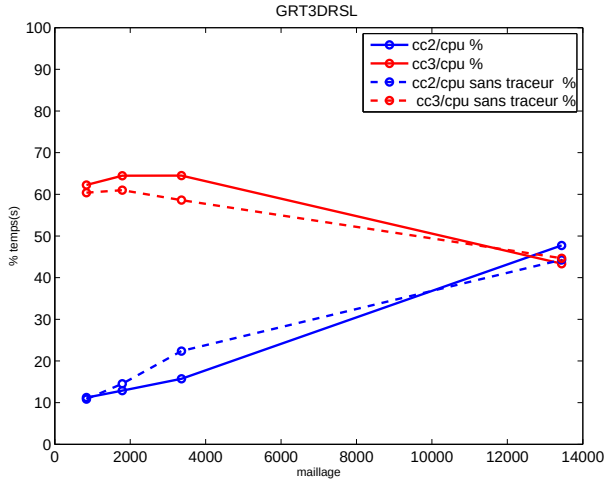

FIGURE 15: Percentage of CPU time in linear solvings (red,cc3) and factorizations (blue, cc2) versus the mesh size using GRT3DRSL. Solid line : with the first component ; dotted line : without the first component.

solvings and matrix factorizations, for the three versions and for two meshes. We see again the effect of the numerical difficulties at time $t = 0$ and the differences between the three versions.

Whereas the number of factorizations is smaller than the number of sol-

vings, the CPU time does not behave in the same way. For the intermediate mesh, facotrization time is smaller than solving time but it becomes larger than solving time for the fine mesh. Because the algorithmic complexity of the factorization is higher, the CPU time increases much faster when the mesh is refined.

This is also illustrated by Figure 15, where we plot the percentage of time spent in linear steps in function of the mesh size, measured by the number of cells. These percentages are computed versus the total CPU time, at the end of the simulations. Computations are done here with the version without logarithms (GRT3DRSL), with and without the first component.

Factorization time becomes relatively more important as the mesh size increases and eventually the lines intersect roughly at the size of the fine mesh. It can also be noted that the addition of both percentages increases with the mesh size. For the fine mesh, more than 90% of CPU time is spent in the Newton's iterations. Therefore, it is really important to reduce the number of iterations and their computational cost.

5 Concluding remarks

In this paper, we have proposed a global approach for simulating reactive transport equations, where transport is coupled with geochemistry. The global method is based on a DAE formulation of the semi-discrete system obtained after space discretization. An implicit time scheme ensures stability and provides an adaptive time step with an adaptive update of the Jacobian matrix. This feature is very efficient as illustrated in our numerical results with the MoMaS benchmark. In order to use this adaptive time scheme, we keep the differential variables, but we eliminate them at the linear level, in order to reduce the system size. This is also very efficient as demonstrated in our results. We could also apply the substitution at the nonlinear level [9, 17]. In the MoMaS benchmark, some concentrations are set to 0 at the intial time and at inflow boundaries. When using logarithmic variables and very small initial concentrations instead of 0, this leads to ill-conditioned systems. It appears that it is more efficient to use nonlogarithmic variables, at least for the test case studied here.

We use a sparse direct solver which first factorizes the Jacobian matrix, then solves two triangular systems. This second step has a much smaller complexity than the first one. Thanks to the adaptive update of the Jacobian, the computational cost of the factorization remains low for the meshes considered here. However, it is clear that this cost will eventually dominate for larger systems. Therefore, we investigate parallel iterative solvers in order to tackle 3D

problems [16].

The test case considered here defines chemistry at equilibrium, without precipitation or dissolution. These reactions are very challenging because minerals can appear and disappear. We study some mathematical issues of this problem [15]. We also plan to include kinetic reactions.

Acknowledgements

This work was partly funded by a grant from ANDRA and by a grant from ANR (H2MNO4 project).

RÉFÉRENCES

[1] Laila Amir and Michel Kern. A global method for coupling transport with chemistry in heterogeneous porous media. *Computational Geosciences*, 14 :465–481, 2010.

[2] J. Carrayrou, J. Hoffmann, P. Knabner, S. Krautle, C. de Dieuleveult, J. Erhel, J. Van der Lee, V. Lagneau, K.U. Mayer, and K.T.B. MacQuarrie. Comparison of numerical methods for simulating strongly non-linear and heterogeneous reactive transport problems. the momas benchmark case. *Computational Geosciences*, 14(3) :483–502, 2010.

[3] JÃ©rÃ´me Carrayrou. Looking for some reference solutions for the reactive transport benchmark of momas with specy. *Computational Geosciences*, 14 :393–403, 2010.

[4] JÃ©rÃ´me Carrayrou, Michel Kern, and Peter Knabner. Reactive transport benchmark of momas. *Computational Geosciences*, 14 :385–392, 2010.

[5] T. Davis. Algorithm 832 : Umfpack, an unsymmetric-pattern multifrontal method. *ACM Transactions on Mathematical Software*, 30 :196–199, 2004.

[6] C. de Dieuleveult. *Un modÃ¨le numÃ©rique global et performant pour le couplage gÃ©ochimie-transport*. PhD thesis, University of Rennes 1, December 2008.

[7] C. de Dieuleveult and J. Erhel. A global approach to reactive transport : application to the momas benchmark. *Computational Geosciences*, 14(3) :451–464, 2010.

[8] C. de Dieuleveult, J. Erhel, and M. Kern. A global strategy for solving reactive transport equations. *Journal of Computational Physics*, 228 :6395–6410, 2009.

[9] J. Erhel, S. Sabit, and C. de Dieuleveult. *Computational Science, Engineering and Technology Series*, volume 31, chapter Solving Partial Differential Algebraic Equations and Reactive Transport Models, pages 151–169. Saxe-Coburg Publications, 2013.

[10] A.W. Harbaugh, E.R. Banta, M.C. Hill, and M.G. McDonald. MODFLOW-2000, the U.S. geological survey modular ground-water model – user guide to modularization concepts and the ground-water flow process. Open-File Report 00-92, U.S. Geological Survey, 2000.

[11] A. C. Hindmarsh, P. N. Brown, K. E. Grant, S. L. Lee, R. Serban, D. E. Shumaker, , and C. S. Woodward. SUNDIALS : Suite of nonlinear and differential/algebraic equation solvers. *ACM Transactions on Mathematical Software*, 31 :363–396, 2005. Also available as LLNL technical report UCRL-JP-200037.

[12] Joachim Hoffmann, Serge Krautle, and Peter Knabner. A parallel global-implicit 2-d solver for reactive transport problems in porous media based on a reduction scheme and its application to the momas benchmark problem. *Computational Geosciences*, 14 :421–433, 2010.

[13] Vincent Lagneau and Jan Lee. Hytec results of the momas reactive transport benchmark. *Computational Geosciences*, 14 :435–449, 2010.

[14] K.Ulrich Mayer and KerryT.B. MacQuarrie. Solution of the momas reactive transport benchmark with min3p - model formulation and simulation results. *Computational Geosciences*, 14 :405–419, 2010.

[15] T. Migot and J. Erhel. Analyse mathÃ©matique de modÃ¨les gÃ©ochimiques. Technical report, Inria, 2014.

[16] F. Pacull, P.M. Gibert, S. Sabit, J. Erhel, and D. Tromeur-Dervout. Parallel preconditioners for 3d global reactive transport. In *Parallel CFD 2014*, Trondheim, Norway, May 2014. invited keynote lecture.

[17] Souhila Sabit. *Les mÃ©thodes numÃ©riques de transport rÃ©actif*. PhD thesis, University of Rennes, May 2014.

[18] C. Zheng and P. Wang. MT3DMS : a modular three-dimensional multi-species model for simulation of advection, dispersion and chemical reactions of contaminants in groundwater systems : documentation and user's guide. Serdp-99-1, U.S. Army Engineer Research and Development Center, 1999.